C Journal of Carbon Research

MDPI

Article

Brewer's Spent Grain Biochar: Grinding Method Matters

Arvind K. Bhakta [1,2,*], Youssef Snoussi [1], Mohamed El Garah [3,4], Souad Ammar [1,*] and Mohamed M. Chehimi [1,*]

1 ITODYS (UMR 7086), CNRS, Université Paris Cité, 75013 Paris, France
2 Department of Chemistry, St. Joseph's College, Bangalore 560027, India
3 LASMIS, Antenne de Nogent—52, Pôle Technologique de Sud—Champagne, 52800 Nogent, France
4 Nogent International Center for CVD Innovation (NICCI), LRC CEA-LASMIS, Pôle Technologique de Sud-Champagne, 52800 Nogent, France
* Correspondence: arvind-kumar.bhakta@u-paris.fr (A.K.B.); ammarmer@univ-paris-diderot.fr (S.A.); mohamed.chehimi@cnrs.fr (M.M.C.)

Abstract: The present work is based on the principle of biomass waste valorization. Brewer's spent grains (BSG) come from breweries as by-products. Their huge amount of production on an industrial scale should focus our attention on their valorization, which creates challenges as well as opportunities. One way to valorize BSG by-products is to convert them into biochar, a functional material with multiple potential applications. With an emphasis on sustainable development and the circular economy, in this work, we focused on a comparative study of the different mechanical processes of BSG grinding and their effect on the resulting biochar formed after pyrolysis. Home appliances such as blenders, coffee mills, and mortar and pestles were used for this purpose. FESEM images confirmed the successful creation of five different morphologies from the same BSG under the same pyrolysis conditions. Interestingly, a novel Chinese tea leaf egg-like biochar was also formed. It was found that a series of physical pretreatments of the biomass resulted in the reduced roughness of the biochar surface, i.e., they became smoother, thus negatively affecting the quality of the biochar. XRD revealed that the biomass physical treatments were also reflected in the crystallinity of some biochar. Via a Raman study, we witnessed the effect of mechanical pressure on the biomass for affecting the biochar features through pressure-induced modifications of the biomass's internal structure. This induced enhanced biochar graphitization. This is a good example of the role of mechanochemistry. DSC revealed the thermochemical transformation of the five samples to be exothermic reactions. This study opens up an interesting possibility for the synthesis of biochar with controlled morphology, crystallinity, degree of graphitization, and heat capacity.

Keywords: brewer's spent grain; biochar; mechanochemistry; graphitization; Chinese tea leaf egg morphology; morphological development processes; waste to wealth

Citation: Bhakta, A.K.; Snoussi, Y.; Garah, M.E.; Ammar, S.; Chehimi, M.M. Brewer's Spent Grain Biochar: Grinding Method Matters. *C* **2022**, *8*, 46. https://doi.org/10.3390/c8030046

Academic Editors: Dimitrios Kalderis and Salvador Ordóñez García

Received: 4 July 2022
Accepted: 9 September 2022
Published: 15 September 2022

1. Introduction

The total number of electrons in a carbon atom is six. Out of this, four valence electrons (outermost shell) contribute to the physico-chemical properties of carbon-based materials. Due to their ability to participate in sp, sp^2, and sp^3 hybridization, they exist in different allotropic forms [1]. Biomass-derived biochar using thermochemical processes has been a hot topic of research in recent years due to its amazing properties [2] including porosity, ultra-high specific surface area [3], and thermal conductivity [4]. Biochar is cost-effective and eco-friendly, which makes it a perfect candidate for a plethora of potential applications [5–7], including soil amendment and water retention, pollutant adsorption [8,9], sensing, and electrochemistry [10]. More generally, biochar contributes to the speeding up of the vision of the circular bioeconomy [11].

A literature survey revealed that the field of biochar has progressed at a remarkable pace since 1999. This 23-year period can be divided into three time zones: before 2009

(initial budding), 2009–2015 (primary growth), and after 2015 (fast progress) [12]. In the current era, due to the importance of biochar, their utilization in urban areas and potential effects have been investigated [13]. Brewer's spent grain (BSG) is a major by-product of beer production and represents a large portion of waste generated after the brewing process [14]. Due to its techno-economic importance [15], BSGs are exploited for different purposes such as biogas and biochar production, the removal of pollutants, the extraction of polyphenols and other compounds, animal nutrition, and for use in fertilizers, to name but a few [16]. A schematic representation of BSG production and valorization is shown in Figure 1. BSGs are rich in fibre (70%) and protein (20%) and their chemical compositions differ depending on the (a) harvest time, (b) kind of barley, (c) malting and mashing procedure, and (d) adjunct used during the brewing process [17].

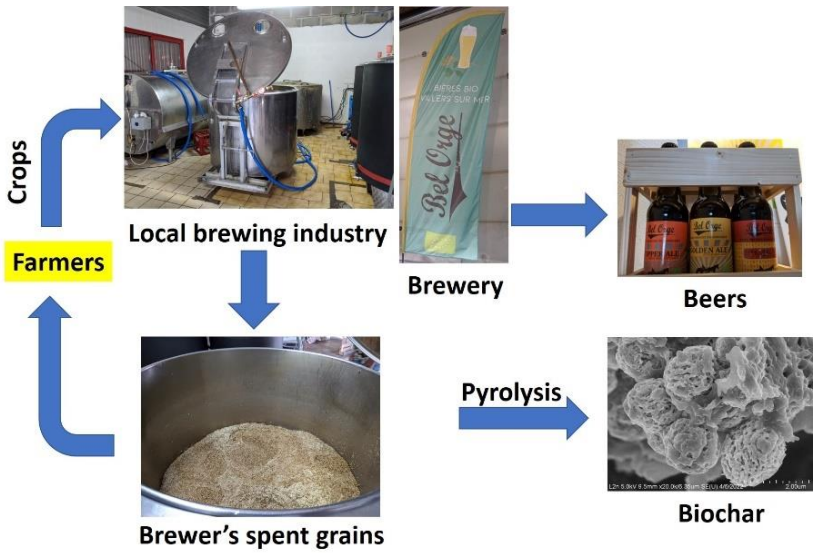

Figure 1. Pictorial representation of the brewing industry, generation of BSGs and their valorization.

The surface morphology, particle size, and porosity of biochar are related to its important features such as its water-holding capacity [18], sorption and cation exchange capacity, energy storage, and immobilization and dispersion of nanocatalysts [19]. This creates a need for the morphological development process. In the literature, there are different methods to tune surface morphology as well as porosity [19]. Mainly, the studies are related to changes in the pyrolysis parameters [20], biomass nature [21], chemical treatment [22], presence of a catalyst [23] or catalyst precursor [24], etc. Even the vacuum freeze-drying procedure [25] could affect the biochar surface morphology. Interestingly, biomass blending affects biochar quality [26].

Pressure engineering is one of the most important techniques used to tune the morphology of biochar. Maliutina et al. [27] studied the effect of pressurized entrained flow pyrolysis. It is well-known that lignocellulosic biomass transformation into fuels and chemicals is difficult due to its rigid structure. In this regard, pretreatment is important because it breaks and eliminates the lignin part of the biomass. This results in changes in the cellulose crystalline structure, which causes cellulose and hemicellulose to be more prone to catalyzed reactions [28,29]. There are plenty of pretreatments reported in the literature for this purpose such as alkaline, hydrothermal, acidic [30,31], metal salts [32], ozonolysis [33], and microwave irradiation [34]. Of these, the majority of treatments are of the alkali or acidic types. Unfortunately, they are less eco-friendly, time-consuming, and produce lots of wastewater. In the context of mechanochemistry, ball milling has been found to be very efficient [35], although it requires high energy. We focused on the importance of home appliances including mortar and pestles for the mechanochemical-induced graphitization of biochar derived from brewing industry waste.

In the present work, we introduced an interesting comparative study involving the production of five biochar surface morphologies using the same BSG under the same pyrolysis conditions but using different grinding techniques for the starting biomass. For this purpose, three different kinds of home appliances (blenders, coffee mills, and mortar and pestles) were used. There were also variations in crystallinity, heat capacity, and the degree of graphitization observed in some samples. Mortar and pestle grinding resulted in an interestingly high degree of graphitization. This work did not require a sophisticated commercially available grinding method for the lab-scale preparation. To the best of our knowledge, no such studies have yet been carried out.

2. Materials and Methods

2.1. Chemicals

Distilled water was used to prepare a BSG smoothie. BSG was gifted from Bel Orge brewery, Villers-sur-Mer 14640, Calvados, Normandy, France (49.32276, 0.01427). We worked on the BSG by-products of lager beer (mixture of malts: barley malt and wheat malt).

2.2. Apparatuses

A blender (Proline, BLS700 model, 700 W, Darty & Fils, Ivry-sur-Seine, F-94200, France), coffee mill/grinder (Duronic), and porcelain mortar and pestle were the home appliances used to process the BSG biomass. The XRD study was carried out using the X'Pert PRO PANalytical instrument. The tube current and operating voltage were maintained at 40 kV and 40 mA, respectively. FESEM was operated at an accelerating voltage of 5 kV and an emission current of 10 µA, with a working distance (WD) of 4.2 mm. An image was taken of a sample that was prepared by pressing a small quantity of biochar material on carbon tape pasted on the sample holder. The excess powder was removed by balloon blowing. EDX was performed on a ZEISS Gemini SEM 360. For this purpose, the biochar sample was dispersed in ethanol and drop-cast onto a silicon plate and dried. RAMAN analysis was performed on a Horiba HR 800 spectrometer. TGA analysis was performed in air from RT to 800 °C at a heating rate of 10 °C/min using a SETARAM instrument (Labsys Evo model). XPS characterization was performed on a Thermo Scientific K Alpha+ apparatus. Pass energy was maintained at 200 eV for the survey scan (step size = 1 eV) and 80 eV for the high-resolution spectra (step size = 0.1 eV).

2.3. Synthesis of Brewer's Spent Grain Biochar

The schematic representation of the synthesis procedure is clearly illustrated in Figure 2. First, the bulk amount of brewer's spent grain biomass from the stock was washed 2 times with tap water, followed by two rounds of washings using distilled water (washed BSG). Then, 175 mL of washed BSG measured using a beaker was added to a blender along with 175 mL of distilled water. It was blended for 2 min on speed setting 5. It was observed that the mixture was very thin. Further, half of the earlier amount was added and blended for 2 more minutes at the same speed. This process resulted in a mixture that looked like a BSG "smoothie", containing 262.5 mL BSG approx. + 175 mL distilled water approx. Ultimately, the biomass-to-water ratio was 1.5: 1. After drying in an oven at an initial 60 °C followed by 100 °C, the BSG "smoothie" formed pellets and was labelled as BSG-SP. These pellets were ground using a coffee mill for 2 min and called BSG-SPCM. The second portion of the washed BSG was dried (BSG-W). It was then ground using a coffee mill (BSG-CM) and another half was subjected to mortar and pestle grinding (BSG-MP) for 30 min. All 5 samples BSG-W, BSG-SP, BSG-SPCM, BSG-CM, and BSG-MP were subjected to pyrolysis and the obtained biochar were referred to as B-W, B-SP, B-SPCM, B-CM, and B- MP, respectively. The parameters chosen for carrying out pyrolysis were as follows: type of method: P10 KOH Free, N_2 flow rate = 1 L/min, ramp = 20 °C/min, temperature = 500 °C, residence time = 1 h, and cooling time = 1 h. This pyrolysis protocol was chosen because it ensures a porous structure [19] and a reduced amount of polycyclic aromatic hydrocarbons (PAHs). Indeed, it is important to note that (PAHs) are normally produced during pyrolysis. These hydrophobic organic compounds

are carcinogenic and could be hazardous pollutants for human beings if they are released from the biochar into the soil and groundwater through rain, irrigation, and root exudates [36–40]. Usually, high-temperature pyrolysis (600–800 °C) yields biochar exceeding the maximum permitted limit of PAH content (12 mg/Kg) [41]. In contrast, biochar synthesized at 500 °C usually has a lower PAH content (483–2100 µg/Kg) [40].

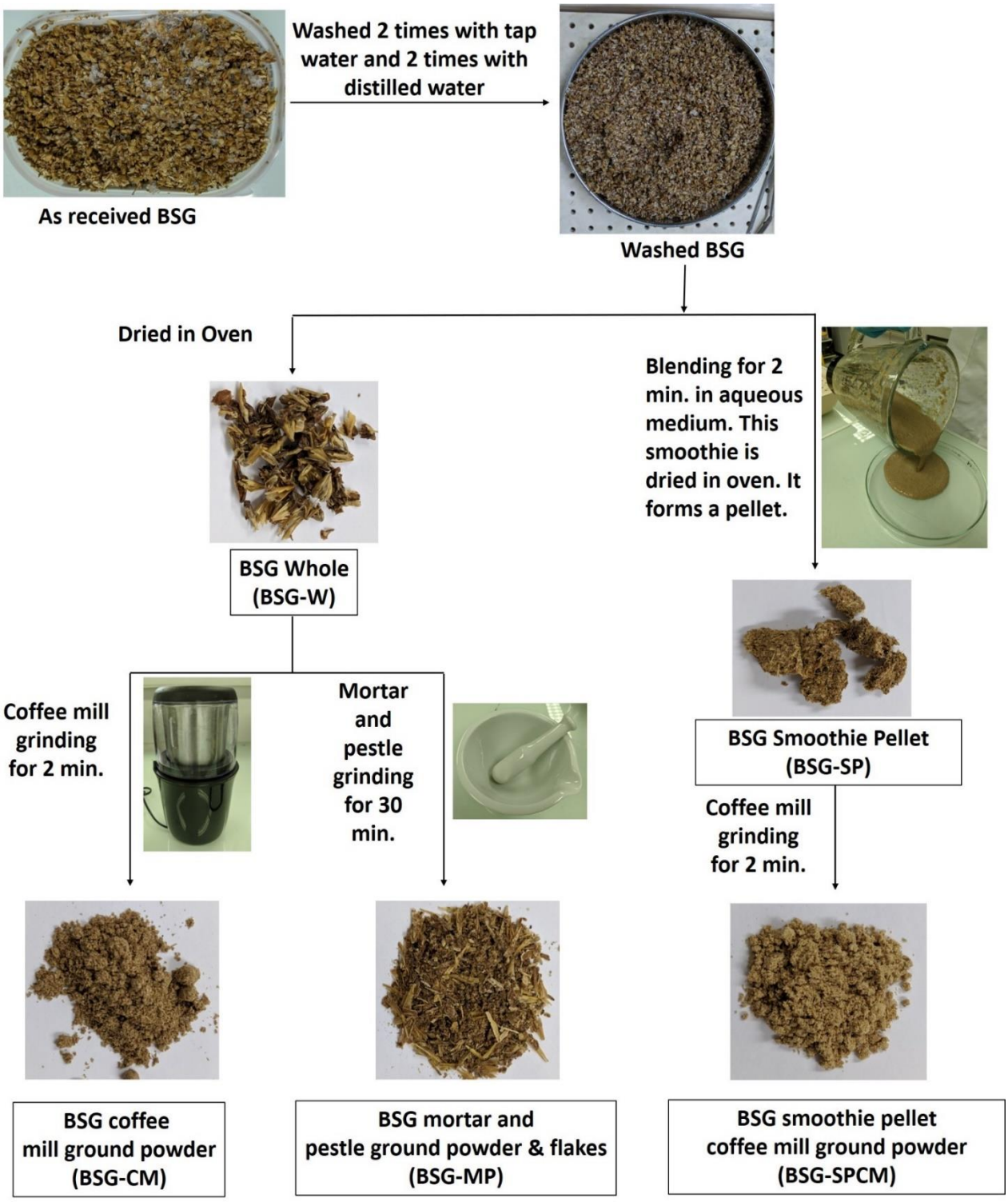

Figure 2. Schematic representation of the procedure to create different samples from the same biomass.

The digital photographs of the different biochar are shown in Figure 3. As the B-SPCM and B-CM biochar samples were found to be dense and molded by the boat-shaped crucible, they were ground using a mortar and pestle. All other biochar samples were tested as prepared without any grinding.

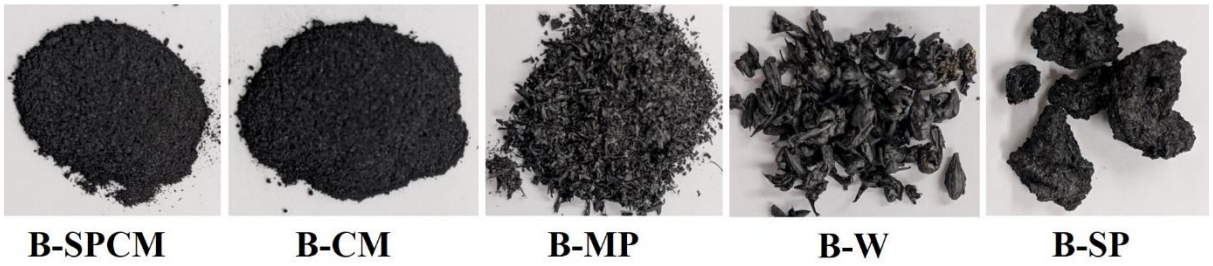

Figure 3. The photo of different textures of the biochar products formed.

The percentage yield was calculated using the formula below.

$$\% \text{ Yield calculated} = (\text{weight of biochar}/\text{weight of biomass}) \times 100 \quad (1)$$

Table 1 reports the amount of biomass taken, the obtained biochar, and the corresponding percentage yield.

Table 1. Summary of the weight of biomass, biochar, and obtained % yield.

Biomass	Weight of Biomass	Biochar	Weight of Biochar	% Yield
BSG-SPCM	5.8096	B-SPCM	1.6226	27.9%
BSG-CM	3.7843	B-CM	1.0893	28.8%
BSG-MP	3.2917	B-MP	0.9337	28.4%
BSG-W	2.0717	B-W	0.6126	29.6%
BSG-SP	2.8120	B-SP	0.8026	28.5%

3. Results and Discussions

3.1. Surface Chemical Composition of Biochar

The elemental compositions derived from the XPS are reported in Table 2 and the corresponding survey spectra are given in Figure 4. It is clear that the major elements present at the surface of the biochar samples are carbon, oxygen, nitrogen, and phosphorous. Silica was detected at trace levels.

Table 2. XPS atomic percentage composition of various biochar samples.

Sample	C	O	N	P	Si	Ca
B-SPCM	80.1	12.1	4.58	1.82	1.25	0.14
B-CM	78.2	13.2	3.74	2.39	1.35	1.16
B-MP	82.1	11.3	3.83	1.25	1.56	-
B-W	78.5	13.3	3.76	2.16	1.39	0.93
B-SP	78.3	13.5	3.80	1.46	2.27	0.61

3.2. Crystallinity of Biochar

The XRD technique was utilized to investigate the crystallinity of the sample. The obvious and broad peaks (Figure 5) observed at $2\theta = 25^{\circ}$ indicate developed turbostratic crystallites in an amorphous matrix [42]. The B-SPCM and B-CM patterns are comparatively less sharp than those of the B-MP, B-W, and B-SP biochar samples. One could hypothesize that pyrolysis of their respective BSG precursors resulted in less crystalline biochar than the non-powdered biomass. This means that the initial texture of the biomass is decisive to

the crystallinity of the produced biochar since the same pyrolysis conditions were set up for the five BSG samples.

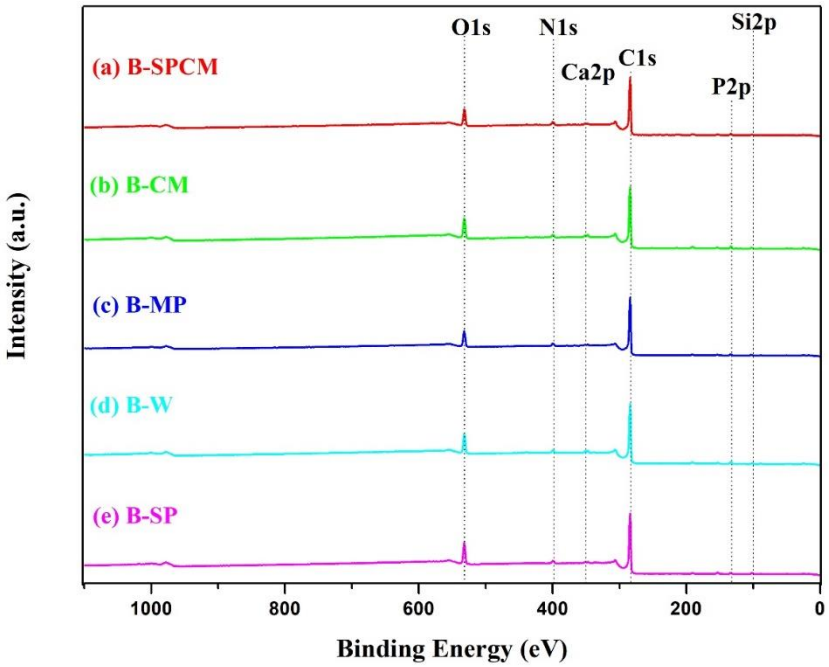

Figure 4. XPS survey spectra of (**a**) B-SPCM, (**b**) B-CM, (**c**) B-MP, (**d**) B-W, and (**e**) B-SP.

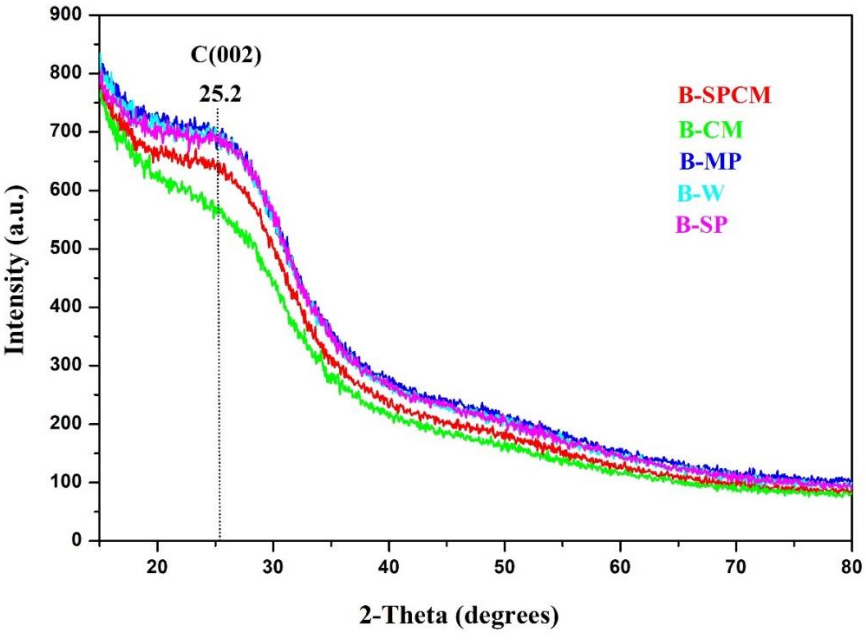

Figure 5. XRD Patterns of B-SPCM, B-CM, B-MP, B-W, and B-SP.

3.3. Morphology of Biochar and Bulk Composition

The surface morphology of the biochar samples was investigated using FESEM. It was observed that the B-SP (Figure 6a,b) and B-SPCM (Figure 6c,d) had a compact surface and porosity was lost to a great extent. Comparatively, B-CM exhibited a compact ball-like structure (appearing as small 1–2 µm-sized carbon particles, which are agglomerated to form a big ball, see Figure 7a,b). In the case of B-MP, an interesting matrix impregnated with a ball-like structure can be seen (Figure 7c–e). Ultimately, B-W showed a novel structure

that resembled a Chinese tea leaf egg (Figure 7f–h). This porosity may be attributed to the mashing [17,43,44] process in the brewery. During brewing, some constituents are removed, which causes shrinkage and creates voids and this forms the basis of the unique biochar formation. It should be noted that generally, the as-received biomass itself is non-homogenous; first, a mixture of grains was received which contained husks and peels and the main grains inside. This caused the appearance of different structures. These are present all around, indicating the homogeneity of the sample and the efficiency of our methodology. From the SEM images, one could anticipate observing distinct textural properties that could be probed by BET surface area measurements [28].

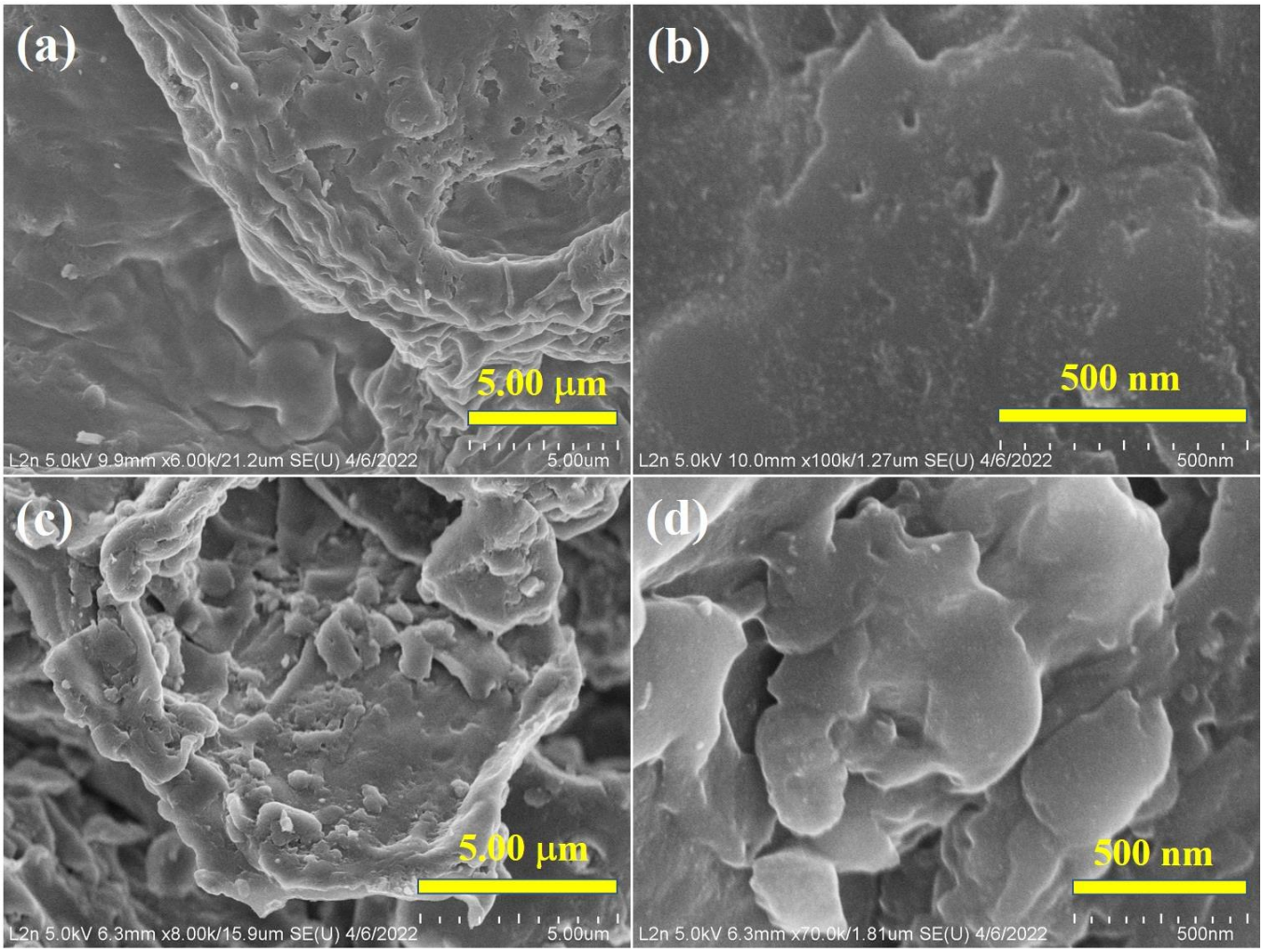

Figure 6. FESEM images of (**a**,**b**) B-SP and (**c**,**d**) B-SPCM.

In order to understand the different morphologies obtained by the different grinding methods, investigating the heat exchange phenomena is highly relevant. Biot number, as well as the convective and diffusive phenomena within the pores of the prepared feedstock, are important aspects in this regard. The retort/sweep gas/partial autothermal pyrolysis processes all behave differently depending on the proportion of heat conduction from the walls in the bulk, inert gas convection and pyrolysis gas convection. These are the key parameters that could lead to different types of biochar production [45–47]. However, these aspects are beyond the aim of the present work and deserve a full, systematic study.

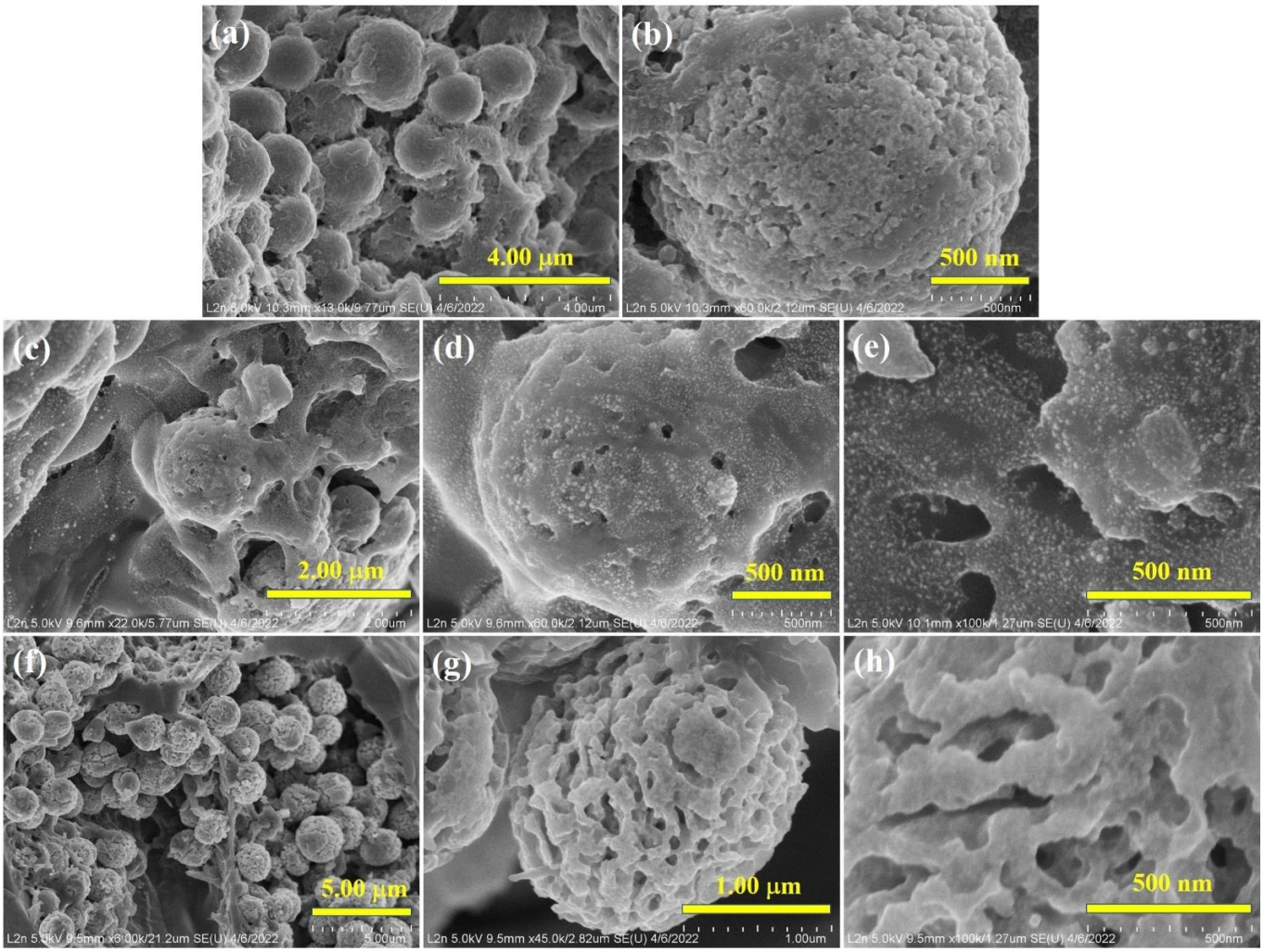

Figure 7. FESEM images of (**a**,**b**) B-CM, (**c**–**e**) B-MP, and (**f**–**h**) B-W.

The EDX mapping was performed in order to determine the elemental compositions and distributions within an analysis depth of 0.02–1.0 µm [48]. Figure 8 displays the EDX mapping, spectrum, and compositions (in at. %) of the B-MP biochar. The different trials of the EDX-determined compositions (in at. %) are reported in Table S1. It was confirmed there was no aluminum, which ruled out any possible incorporation of alumina during the grinding of the BSGs by mortar and pestle. The analysis was performed in different spots showing similar elemental compositions (see caption for Figure 8), suggesting a good homogeneity of the obtained biochar. The EDX mapping shows the homogeneous distribution of all elements on the spotted biochar particle without any noticeable defects. For more accuracy, the whole biochar should be characterized by CHNS elemental analysis. This could, for example, give the H/C atomic ratio, which is intimately correlated with the pyrolysis temperature [49].

3.4. Carbon Skeleton Structure of Biochar

Raman analysis is an important technique for understanding the defective nature of carbonaceous materials and occurrence of aromatic structures [50,51]. The Raman peak fitting (Figure 9) was carried out to understand the quality of the synthesized biochar. Here, there are mostly six components, namely S_L (hydrogen circulation along the periphery of the biochar, S (alkyl–alkyl ether), D (defects, heteroatoms, etc.), V (sp^2 C), G (degree of graphitization), and G_L (carbonyl function) [52–54]. The D/G ratio was calculated by both

peak areas and intensity. In four of the samples, a D/G ratio > 1 indicated a low degree of graphitization and the presence of more defects.

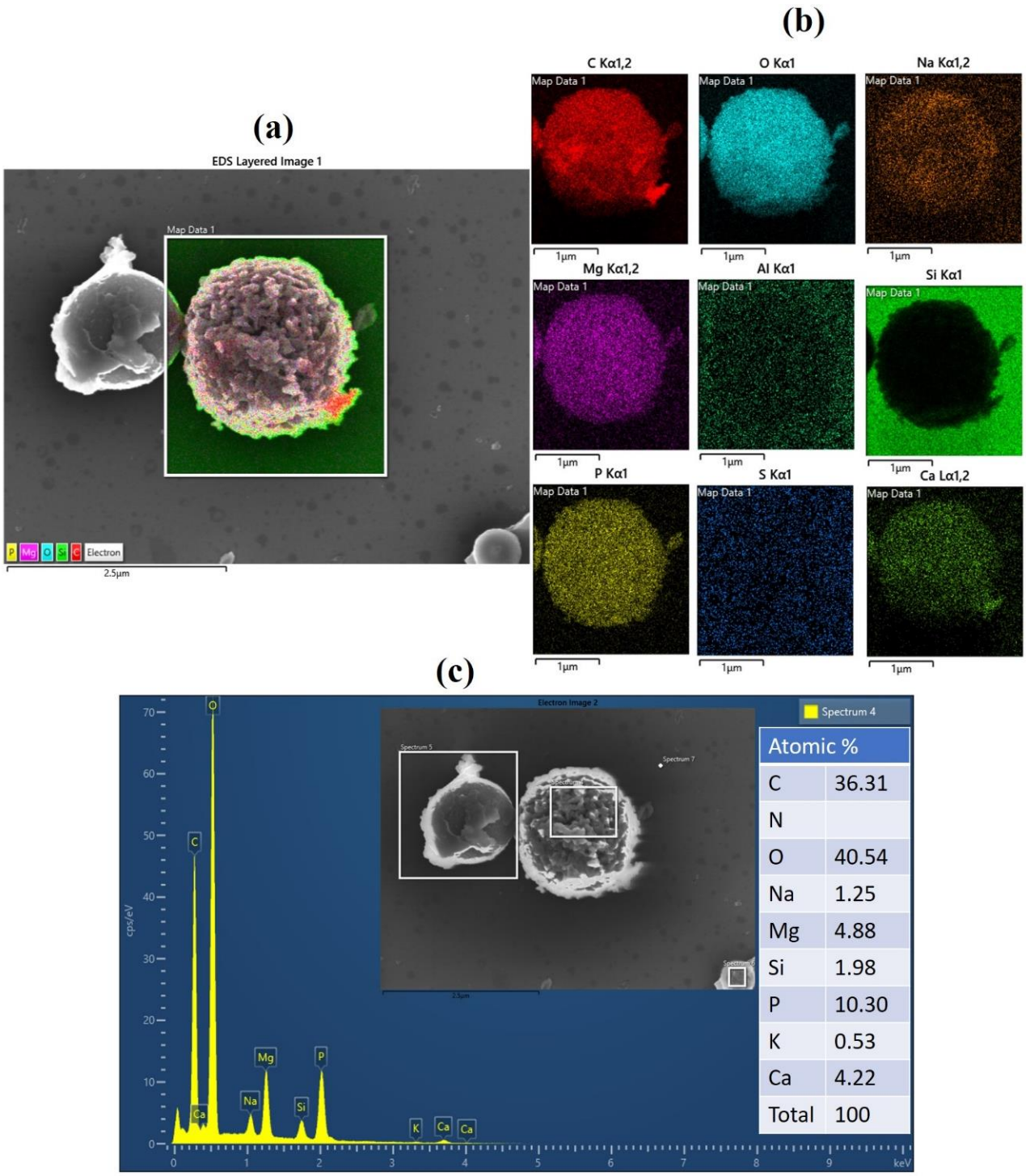

Figure 8. (**a**) FESEM image of B-MP, (**b**) EDX mapping of B-MP, (**c**) EDX spectrum of B-MP (inset: area showing the spectra on which spectrum 4 was performed). (NB: Three different areas were probed and the average composition (in at.%) was as follows: C = 35.0 ± 2.3, O = 39.6 ± 1.9, Na = 1.5 ± 0.8, Mg = 5.2 ± 0.3, Si = 2.7 ± 1.3, P = 11.0 ± 0.6, K= 0.6 ± 0.1, and Ca = 4.5 ± 0.5).

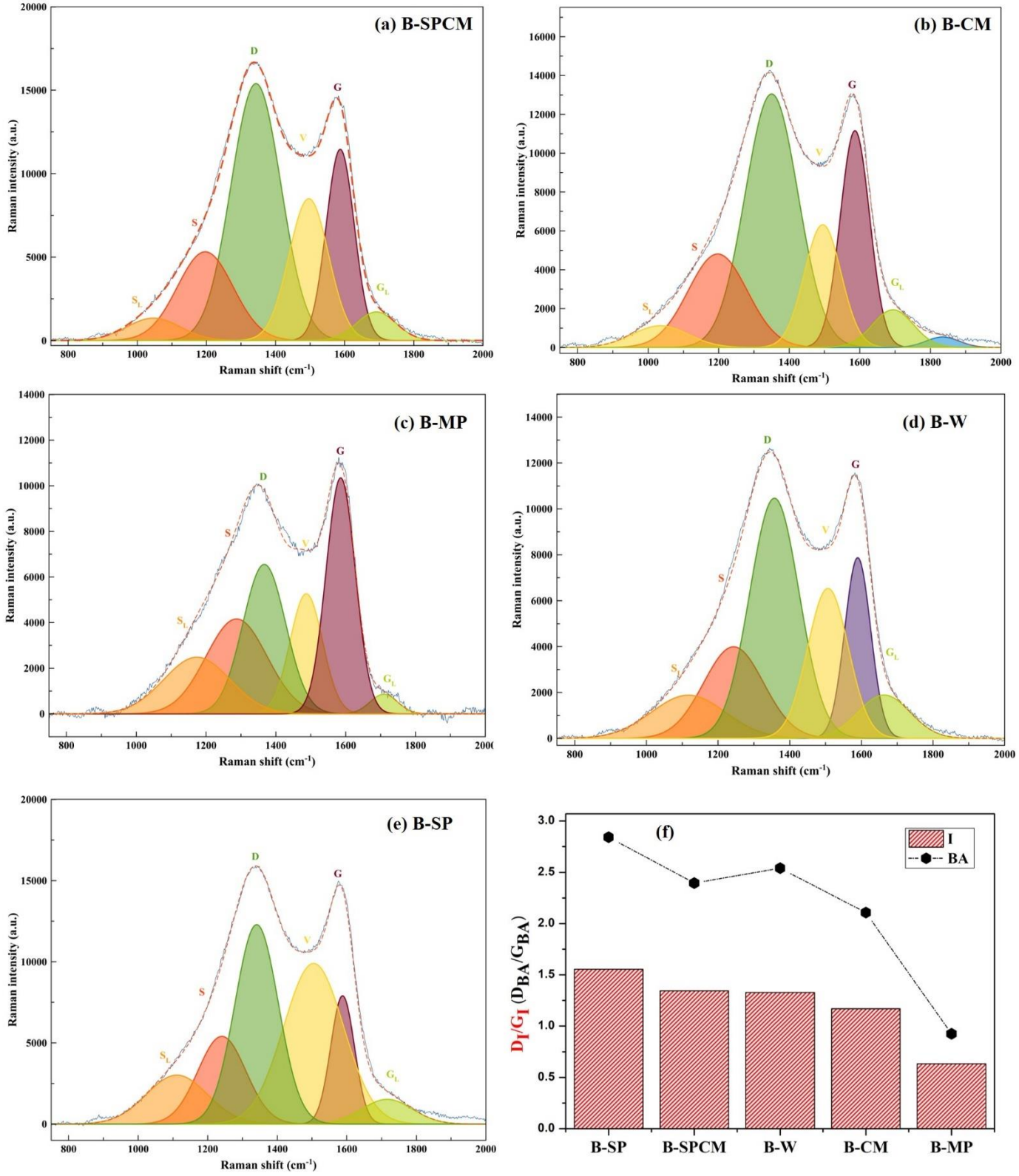

Figure 9. (a–e) Raman peak fitting and (**f**) D/G band intensity and band area ratio.

However, the B-MP biochar exhibited a D/G ratio < 1 indicating a high degree of graphitization as shown in Figure 9c,f. This is clear proof that biomass grinding using a mortar and pestle induced a mechanochemical reaction [27]. Basically, the pretreatment of BSG may result in the reorganization of the internal moieties, hence the obtaining of a more

graphitized structure. It is worth noting that this same B-MP biochar had the highest carbon content as judged from the XPS analysis, a result that parallels the noted graphitization.

3.5. Thermal Stability

The thermal stability analysis of the biochar samples is shown in Figure 10. Figure 10a shows the TGA curves. There are few differences between the TGA thermograms of the five biochars (Figure 10a), which indicates they followed a similar pattern of decomposition. They are mainly categorized into three regions [55,56]: below ~300 °C is attributed to the removal of low-boiling-point organics and the evaporation of moisture; between 300 and 660 °C, the rapid decomposition of the biochar occurs; above 660 °C, the decomposition phenomenon becomes more stabilized; and at At 800 °C, the residual biochar accounts for 20 wt.% of the initial biochar. However, the DSC curves show significant changes, particularly for the B-CM biochar (Figure 10b). The curve shows values on a positive scale, which is an indication of the exothermic process. The amount of heat flow in the different materials is in the order of B-W < B-MP < B-SPCM < B-SP < B-CM. The derivative weight loss curve [57] of the different biochar samples is shown in Figure 10c. The DTG have two important parameters, i.e., T_{ic} (temperature of initial combustion) and T_{mwl} (temperature of maximum weight loss rate) [58]. The T_{mwl} values of the different biochar samples are shown in Figure 10c. B-CM has the highest T_{mwl}, i.e., 543 °C, indicating that it is the most stable biochar.

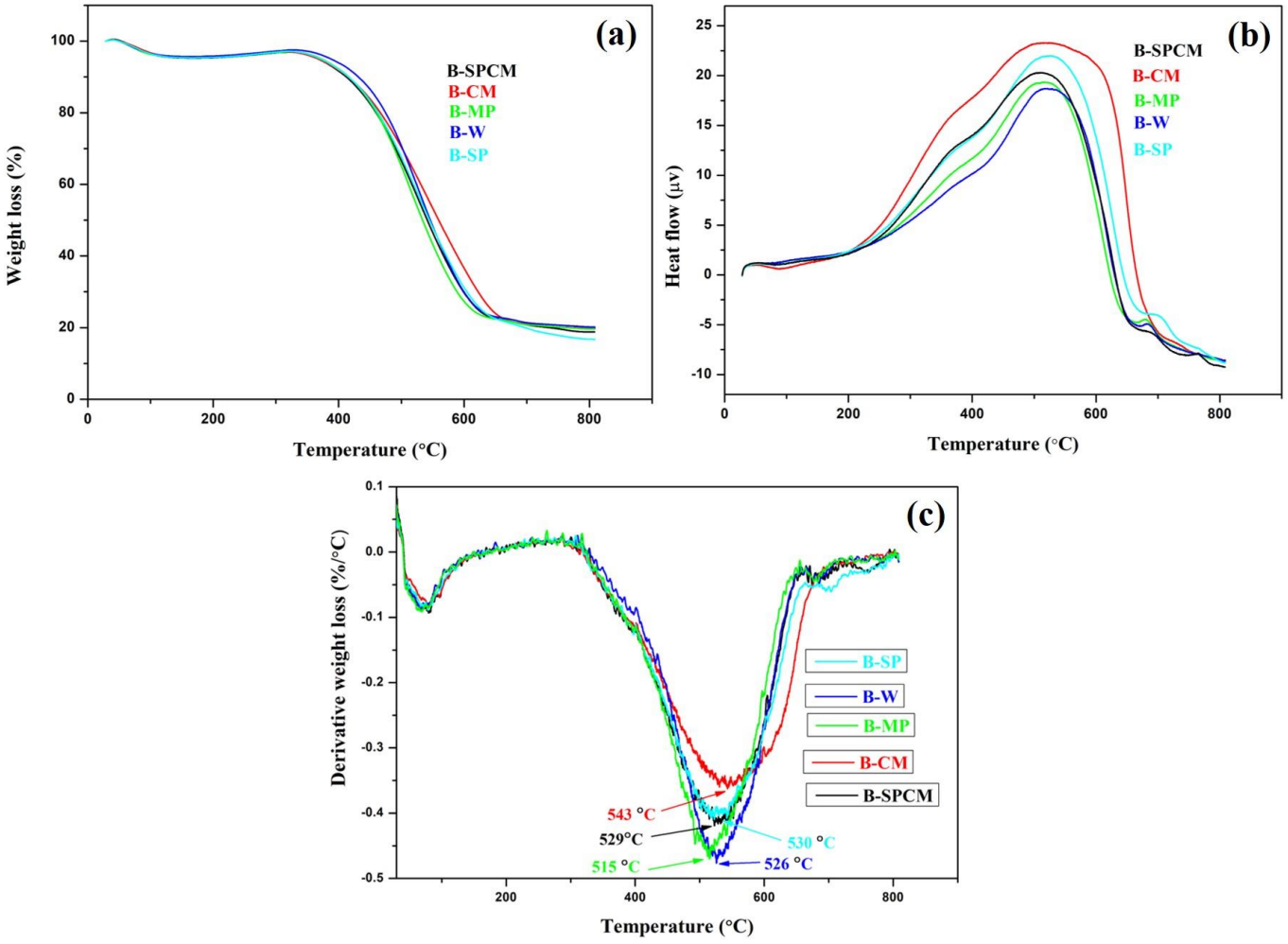

Figure 10. (**a**) TGA, (**b**) DSC, and (**c**) DTG curve of different biochar samples.

4. Conclusions

In this work, we prepared five biochar samples from the same brewer's spent grains (BSGs) that were ground via five different approaches. The comparative study of the different grinding processes revealed that these processes had a major effect on the surface morphology of the biomass-derived biochar. Surprisingly, the harsh mechanical treatment of the initial biomass resulted in less porosity. A novel Chinese tea leaf egg-like structure was found in the biochar derived from the mortar-and-pestle-ground BSG. The grinding method also affected the thermal behavior and the degree of graphitization of the biochar as judged by the change in the D to G Raman band intensity ratio. To sum up, home appliances for treating biomass are a simple procedure and easily available. Mechanochemistry plays an important role in tuning surface morphology. This work provides an interesting perspective in the field of biochar as it conclusively demonstrates the effect of mechanochemistry of the initial biomass on the surface morphology of the resulting biochar. This study was conducted with brewer's spent grains but inspired us to investigate whether it could be extended to other types of agro waste. Research is underway toward this end.

Supplementary Materials: The following supporting information can be downloaded at: https://www.mdpi.com/article/10.3390/c8030046/s1, Table S1: Percentage composition of B-MP obtained through EDX analysis.

Author Contributions: Conceptualization, A.K.B., Y.S. and M.M.C.; methodology, A.K.B., Y.S. and M.M.C.; validation, all authors; formal analysis, A.K.B., Y.S. and M.E.G.; investigation, A.K.B., Y.S. and M.E.G.; resources, A.K.B., M.M.C. and S.A.; data curation, A.K.B.; writing—original draft preparation, A.K.B.; writing—review and editing, all authors; visualization, A.K.B., Y.S. and M.M.C.; supervision, S.A. and M.M.C.; project administration, S.A. and M.M.C.; funding acquisition, A.K.B., S.A. and M.M.C. All authors have read and agreed to the published version of the manuscript.

Funding: This research was funded by the "Bourse Wallonie-Bruxelles International Excellence World (N Imputation—101386, and Article Budgetaire—33.01.00.07)". This work was also supported by the French Ministry of Research. ANR (*Agence Nationale de la Recherche*) and CGI (*Commissariat à l'Investissement d'Avenir*) are gratefully acknowledged for their financial support of this work through Labex SEAM (ANR-11-LABX-086, ANR-11-IDEX-0502) grant and the APC was funded by C-MDPI.

Institutional Review Board Statement: Not applicable.

Informed Consent Statement: Not applicable.

Data Availability Statement: Not applicable.

Acknowledgments: All authors are thankful to the experimental officers at the ITODYS lab for their assistance with the EDX, Raman analysis, TGA and DSC studies, XRD characterization, and XPS surface analysis. Our gratitude is extended to Benoit Boisanfray from Bel Orge brewery for the gift of the brewer's spent grains (Bel Orge is located at 6 Rue des Grives, F-14640 Villers-sur-Mer, Calvados, Normandy, France).

Conflicts of Interest: The authors declare no conflict of interest. The funders and Bel Orge brewery (provider of BSGs) had no role in the design of the study; in the collection, analyses, or interpretation of data; in the writing of the manuscript; or in the decision to publish the results.

References

1. Meunier, V.; Ania, C.; Bianco, A.; Chen, Y.; Choi, G.B.; Kim, Y.A.; Koratkar, N.; Liu, C.; Tascon, J.M.; Terrones, M. Carbon science perspective in 2022: Current research and future challenges. *Carbon* **2022**, *195*, 272–291. [CrossRef]
2. Weber, K.; Quicker, P. Properties of biochar. *Fuel* **2018**, *217*, 240–261. [CrossRef]
3. Dou, S.; Ke, X.; Shao, Z.; Zhong, L.; Zhao, Q.; Zheng, Y.-M. Fish scale-based biochar with defined pore size and ultrahigh specific surface area for highly efficient adsorption of ciprofloxacin. *Chemosphere* **2022**, *287*, 131962. [CrossRef] [PubMed]
4. Xiong, T.; Ok, Y.S.; Dissanayake, P.D.; Tsang, D.C.W.; Kim, S.; Kua, H.W.; Shah, K.W. Preparation and thermal conductivity enhancement of a paraffin wax-based composite phase change material doped with garlic stem biochar microparticles. *Sci. Total Environ.* **2022**, *827*, 154341. [CrossRef]
5. Kumar, A.; Bhattacharya, T.; Mukherjee, S.; Sarkar, B. A perspective on biochar for repairing damages in the soil—plant system caused by climate change—driven extreme weather events. *Biochar* **2022**, *4*, 1–23. [CrossRef]

6. Kasera, N.; Kolar, P.; Hall, S.G. Nitrogen—doped biochars as adsorbents for mitigation of heavy metals and organics from water: A review. *Biochar* **2022**, *4*, 17. [CrossRef]
7. de Gomes, S.C.; Zhou, J.L.; Zeng, X.; Long, G. Water treatment sludge conversion to biochar as cementitious material in cement composite. *J. Environ. Manage.* **2022**, *306*, 114463. [CrossRef]
8. Dewangan, S.; Bhatia, A.K.; Singh, A.K.; Carabineiro, S.A.C. Removal of Hydrophobic Contaminants from the Soil by Adsorption onto Carbon Materials and Microbial Degradation. *J. Carbon Res.* **2021**, *7*, 83. [CrossRef]
9. Peterson, S.C.; Kim, S.; Adkins, J. Surface Charge Effects on Adsorption of Solutes by Poplar and Elm Biochars. *J. Carbon Res.* **2021**, *7*, 11. [CrossRef]
10. Binda, G.; Faccini, D.; Zava, M.; Pozzi, A.; Dossi, C.; Monticelli, D.; Spanu, D. Exploring the Adsorption of Pb on Microalgae-Derived Biochar: A Versatile Material for Environmental Remediation and Electroanalytical Applications. *Chemosensors* **2022**, *10*, 168. [CrossRef]
11. Ghodake, G.S.; Shinde, S.K.; Kadam, A.A.; Saratale, R.G.; Saratale, G.D.; Kumar, M.; Palem, R.R.; L-Shwaiman, H.A.A.; Elgorban, A.M.; Syed, A.; et al. Review on biomass feedstocks, pyrolysis mechanism and physicochemical properties of biochar: State-of-the-art framework to speed up vision of circular bioeconomy. *J. Clean. Prod.* **2021**, *297*, 126645. [CrossRef]
12. Qin, F.; Li, J.; Zhang, C.; Zeng, G.; Huang, D.; Tan, X.; Qin, D.; Tan, H. Biochar in the 21st century: A data-driven visualization of collaboration, frontier identifi cation, and future trend. *Sci. Total Environ.* **2022**, *818*, 151774. [CrossRef] [PubMed]
13. EAzzi, S.; Karltun, E.; Sundberg, C. Life cycle assessment of urban uses of biochar and case study in Uppsala, Sweden. *Biochar* **2022**, *4*, 1–17. [CrossRef]
14. Vieira, M.C.; Brandelli, A.; Thys, R.C.S. Evaluation of the technological functional properties and antioxidant activity of protein hydrolysate obtained from brewers' spent grain. *J. Food Process. Preserv.* **2022**, *46*, e16638. [CrossRef]
15. Allegretti, C.; Bellinetto, E.; Arrigo, P.D.; Griffini, G.; Marzorati, S.; Rossato, L.A.M.; Ruffini, E.; Schiavi, L.; Serra, S.; Strini, A.; et al. Towards a Complete Exploitation of Brewers' Spent Grain from a Circular Economy Perspective. *Fermentation* **2022**, *8*, 151. [CrossRef]
16. Jackowski, M.; Niedzwiecki, Ł.; Jagiełło, K.; Uchanska, O.; Trusek, A. Brewer 's Spent Grains—Valuable Beer Industry By-Product. *Biomolecules* **2020**, *10*, 1669. [CrossRef]
17. Mugoronji, M.; Manyuchi, M.M.; Sukdeo, N.; Stinner, W. Techno-economic assessment for bio coal production from brewers spent grain. *South African J. Chem. Eng.* **2022**, *40*, 1–9. [CrossRef]
18. Batista, E.M.C.C.; Shultz, J.; Matos, T.T.S.; Fornari, M.R.; Ferreira, T.M.; Szpoganicz, B.; de Freitas, R.A.; Mangrich, A.S. Effect of surface and porosity of biochar on water holding capacity aiming indirectly at preservation of the Amazon biome. *Sci. Rep.* **2018**, *8*, 10677. [CrossRef]
19. Leng, L.; Xiong, Q.; Yang, L.; Li, H.; Zhou, Y.; Zhang, W.; Jiang, S.; Li, H.; Huang, H. An overview on engineering the surface area and porosity of biochar. *Sci. Total Environ.* **2021**, *763*, 144204. [CrossRef]
20. Zhao, B.; Connor, D.O.; Zhang, J.; Peng, T.; Shen, Z.; Tsang, D.C.W.; Hou, D. Effect of pyrolysis temperature, heating rate, and residence time on rapeseed stem derived biochar. *J. Clean. Prod.* **2018**, *174*, 977–987. [CrossRef]
21. Suman, S.; Panwar, D.S.; Gautam, S. Surface morphology properties of biochars obtained from different biomass waste. *Energy Sources Part A Recovery Util. Environ. Eff.* **2017**, *39*, 1007–1012. [CrossRef]
22. dos Reis, G.S.; Guy, M.; Mathieu, M.; Jebrane, M.; Lima, E.C.; Thyrel, M.; Dotto, G.L.; Larsson, S.H. A comparative study of chemical treatment by MgCl2, ZnSO4, ZnCl2, and KOH on physicochemical properties and acetaminophen adsorption performance of biobased porous materials from tree bark residues. *Colloids Surf. A Physicochem. Eng. Asp.* **2022**, *642*, 128626. [CrossRef]
23. Tripathi, M.; Sahu, J.N.; Ganesan, P. Effect of process parameters on production of biochar from biomass waste through pyrolysis: A review. *Renew. Sustain. Energy Rev.* **2016**, *55*, 467–481. [CrossRef]
24. Tang, M.; Snoussi, Y.; Bhakta, A.K.; el Garah, M.; Khalil, A.M.; Ammar, S.; Chehimi, M.M. Unusual, hierarchically structured composite of sugarcane pulp bagasse biochar loaded with Cu/Ni bimetallic nanoparticles. *Chemrxiv* **2022**. [CrossRef]
25. Meng, F.; Wang, D. Effects of vacuum freeze drying pretreatment on biomass and biochar properties. *Renew. Energy.* **2020**, *155*, 1–9. [CrossRef]
26. Bhatnagar, A.; Singhal, A.; Tolvanen, H.; Valtonen, K.; Joronen, T.; Konttinen, J. Effect of pretreatment and biomass blending on bio-oil and biochar quality from two-step slow pyrolysis of rice straw. *Waste Manag.* **2022**, *138*, 298–307. [CrossRef]
27. Maliutina, K.; Tahmasebi, A.; Yu, J. Effects of pressure on morphology and structure of bio-char from pressurized entrained- flow pyrolysis of microalgae. *Data Br.* **2018**, *18*, 422–431. [CrossRef]
28. Shen, F.; Xiong, X.; Fu, J.; Yang, J.; Qiu, M.; Qi, X.; Daniel, C.; Tsang, W. Recent advances in mechanochemical production of chemicals and carbon materials from sustainable biomass resources. *Renew. Sustain. Energy Rev.* **2020**, *130*, 109944. [CrossRef]
29. Alvira, P.; Tomás-Pejó, E.; Ballesteros, M.; Negro, M.J. Pretreatment technologies for an efficient bioethanol production process based on enzymatic hydrolysis: A review. *Bioresour. Technol.* **2010**, *101*, 4851–4861. [CrossRef]
30. Ban, S.; Lee, E.; Lim, D.; Kim, I.; Lee, J. Evaluation of sulfuric acid-pretreated biomass-derived biochar characteristics and its diazinon adsorption mechanism. *Bioresour. Technol.* **2022**, *348*, 126828. [CrossRef]
31. Alayont, S.; Kayan, D.B.; Durak, H.; Alayont, E.K.; Genel, S. The role of acidic, alkaline and hydrothermal pretreatment on pyrolysis of wild mustard (Sinapis arvensis) on the properties of bio-oil and bio-char. *Bioresour. Technol. Reports.* **2022**, *17*, 100980. [CrossRef]

32. Garrido, R.A.; Reckamp, J.; Bastian, P.; Hammer, N.H.; Coe, C.G.; Satrio, J.A. Influences of zinc chloride on fast pyrolysis of pinewood. *IOP Conf. Ser. Earth Environ. Sci.* **2022**, *1034*, 012042. [CrossRef]
33. Bhatia, S.K.; Ahuja, V.; Chandel, N.; Gurav, R.; Bhatia, R.K.; Muthusamy, G.; Tyagi, V.K.; Kumar, V.; Pugazendhi, A.; Banu, R.J.; et al. Advances in algal biomass pretreatment and its valorisation into biochemical and bioenergy by the microbial processes. *Bioresour. Technol.* **2022**, *358*, 127437. [CrossRef]
34. Hadiya, V.; Popat, K.; Vyas, S.; Varjani, S.; Vithanage, M.; Gupta, V.K.; Delgado, A.N.; Zhou, Y.; Show, P.L.; Bilal, M.; et al. Biochar production with amelioration of microwave-assisted pyrolysis: Current scenario, drawbacks and perspectives. *Bioresour. Technol.* **2022**, *355*, 127303. [CrossRef] [PubMed]
35. Sitotaw, Y.W.; Habtu, N.G.; Gebreyohannes, A.Y.; Nunes, S.P.; van Gerven, T. Ball milling as an important pretreatment technique in lignocellulose biorefineries: A review. *Biomass Convers. Biorefinery* **2021**, 1–24. [CrossRef]
36. Hung, C.; Chen, C.; Huang, C.; Yang, Y.; Dong, C. Suppression of polycyclic aromatic hydrocarbon formation during pyrolytic production of lignin-based biochar via nitrogen and boron co-doping. *Bioresour. Technol.* **2022**, *355*, 127246. [CrossRef] [PubMed]
37. Shen, X.; Meng, H.; Shen, Y.; Ding, J.; Zhou, H.; Cong, H.; Li, L. A comprehensive assessment on bioavailability, leaching characteristics and potential risk of polycyclic aromatic hydrocarbons in biochars produced by a continuous pyrolysis system. *Chemosphere* **2022**, *287*, 132116. [CrossRef]
38. Qiu, M.; Sun, K.; Jin, J.; Han, L.; Sun, H.; Zhao, Y.; Xia, X.; Wu, F.; Xing, B. Metal/metalloid elements and polycyclic aromatic hydrocarbon in various biochars: The effect of feedstock, temperature, minerals, and properties. *Environ. Pollut.* **2015**, *206*, 298–305. [CrossRef]
39. Zhao, L.; Zhao, Y.; Nan, H.; Yang, F.; Qiu, H.; Xu, X.; Cao, X. Suppressed formation of polycyclic aromatic hydrocarbons (PAHs) during pyrolytic production of Fe-enriched composite biochar. *J. Hazard. Mater.* **2020**, *382*, 121033. [CrossRef]
40. Wang, J.; Odinga, E.S.; Zhang, W.; Zhou, X.; Yang, B.; Waigi, M.G.; Gao, Y. Polyaromatic hydrocarbons in biochars and human health risks of food crops grown in biochar-amended soils: A synthesis study. *Environ. Int.* **2019**, *130*, 104899. [CrossRef]
41. EBC. *European Biochar Certificate—Guidelines for a Sustainable Production of Biochar. Switzerland Version 8E of 1st January 2019*; European Biochar Foundation (EBC): Arbaz, Switzerland, 2017. [CrossRef]
42. Chen, W.; Feng, J.; Liu, S.; Zhang, J.; Cai, Y.; Lv, Z.; Fang, M.; Tan, X. A green and economical MgO/biochar composite for the removal of U (VI) from aqueous solutions. *Chem. Eng. Res. Des.* **2022**, *180*, 391–401. [CrossRef]
43. Jin, Z.; Lan, Y.; Ohm, J.; Gillespie, J.; Schwarz, P.; Chen, B. Physicochemical composition, fermentable sugars, free amino acids, phenolics, and minerals in brewers' spent grains obtained from craft brewing operations. *J. Cereal Sci.* **2022**, *104*, 103413. [CrossRef]
44. Endres, F.; Prowald, A.; Elisabeth, U.; Fittschen, A.; Hampel, S.; Oppermann, S.; Jacob, F.; Hutzler, M.; Laus, A.; Methner, Y.; et al. Constant temperature mashing at 72 °C for the production of beers with a reduced alcohol content in micro brewing systems. *Eur. Food Res. Technol.* **2022**, *248*, 1457–1468. [CrossRef]
45. Peterson, C.A.; Hornbuckle, M.K.; Brown, R.C. Biomass pyrolysis devolatilization kinetics of herbaceous and woody feedstocks. *Fuel Process. Technol.* **2022**, *226*, 107068. [CrossRef]
46. Agar, D.A.; Kwapinska, M.; Leahy, J.J. Pyrolysis of wastewater sludge and composted organic fines from municipal solid waste: Laboratory reactor characterisation and product distribution. *Sustain. WASTE Manag.* **2018**, *25*, 35874–35882. [CrossRef]
47. Pecha, M.B.; Thornburg, N.E.; Peterson, C.A.; Crowley, M.F.; Gao, X.; Lu, L.; Wiggins, G.; Brown, R.C.; Ciesielski, P.N. Impacts of Anisotropic Porosity on Heat Transfer and Off-Gassing during Biomass Pyrolysis. *Energy Fuels.* **2021**, *35*, 20131–20141. [CrossRef]
48. Gibson, L.T. Archaeometry and Antique Analysis | Metallic and Ceramic Objects. *Encycl. Anal. Sci. Second Ed.* **2005**, 117–123. [CrossRef]
49. Xiao, X.; Chen, Z.; Chen, B. H/C atomic ratio as a smart linkage between pyrolytic temperatures, aromatic clusters and sorption properties of biochars derived from diverse precursory materials. *Sci. Rep.* **2016**, *6*, 22644. [CrossRef]
50. Tran, H.N.; Tomul, F.; Ha, N.T.H.; Nguyen, D.T.; Lima, E.C.; Le, G.T.; Chang, C.-T.; Masindi, V.; Woo, S.H. Innovative spherical biochar for pharmaceutical removal from water: Insight into adsorption mechanism. *J. Hazard. Mater.* **2020**, *394*, 122255. [CrossRef]
51. Mcdonald-wharry, J. 2013–2014 Survey of Chars Using Raman Spectroscopy. *J. Carbon Res.* **2021**, *7*, 63. [CrossRef]
52. Inoue, J.; Yoshie, A.; Tanaka, T.; Onji, T.; Inoue, Y. Disappearance and alteration process of charcoal fragments in cumulative soils studied using Raman spectroscopy. *Geoderma* **2017**, *285*, 164–172. [CrossRef]
53. Pusceddu, E.; Montanaro, A.; Fioravanti, G.; Santilli, S.F.; Foscolo, P.U.; Criscuoli, I.; Raschi, A.; Miglietta, F. Comparison between Ancient and Fresh Biochar Samples, A Study on The Recalcitrance of Carbonaceous Structures During Soil Incubation. *Int. J. New Technol. Res.* **2017**, *3*, 39–46.
54. Feng, D.; Zhao, Y.; Zhang, Y.; Sun, S.; Gao, J. Steam Gasification of Sawdust Biochar Influenced by Chemical Speciation of Alkali and Alkaline Earth Metallic Species. *Energies* **2018**, *11*, 205. [CrossRef]
55. Wang, W.; Bai, J.; Lu, Q.; Zhang, G.; Wang, D.; Jia, J.; Guan, Y.; Yu, L. Pyrolysis temperature and feedstock alter the functional groups and carbon sequestration potential of Phragmites australis—and Spartina alterniflora-derived biochars. *GCB Bioenergy* **2021**, *13*, 493–506. [CrossRef]
56. Cui, B.; Chen, Z.; Guo, D.; Liu, Y. Investigations on the pyrolysis of microalgal-bacterial granular sludge: Products, kinetics, and potential mechanisms. *Bioresour. Technol.* **2022**, *349*, 126328. [CrossRef] [PubMed]

57. Chen, Y.; Cui, Z.; Ding, H.; Wan, Y.; Tang, Z.; Gao, J. Cost-Effective Biochar Produced from Agricultural Residues and Its Application for Preparation of High Performance Form-Stable Phase Change Material via Simple Method. *Int. J. Mol. Sci.* **2018**, *19*, 3055. [CrossRef] [PubMed]
58. Riva, L.; Cardarelli, A.; Andersen, G.J.; Buø, T.V.; Barbanera, M.; Bartocci, P.; Fantozzi, F.; Nielsen, H.K. On the self-heating behavior of upgraded biochar pellets blended with pyrolysis oil: Effects of process parameters. *Fuel* **2020**, *278*, 118395. [CrossRef]